Proceedings of the 5th WSEAS International Conference on Signal Processing, Istanbul, Turkey, May 27-29, 2006 (pp24-29)

Locating mines in SAR imagery using change detection methods

Maria Tates[a,b], Nasser M. Nasrabadi[a], Heesung Kwon[a]
[a]U.S. Army Research Laboratory, 2800 Powder Mill Rd., Adelphi, MD 20783
[b]Morgan State University, 5200 Perring Pkwy., Baltimore, MD 21251

Abstract: - In this paper we present several methods for change detection in a pair of multi-look synthetic aperture radar (SAR) images of the same scene. We implement and compare several techniques which vary in complexity. Among the simple methods that are implemented are differencing, Euclidean distance, and image ratioing. These methods require minimal processing time, with little computational complexity, and incorporate no statistical information. We also implemented methods which incorporate second order statistic calculations in making a change decision in efforts to mitigate false alarms arising from the speckle noise, misregistration errors, and nonlinear variations in SAR images. These methods include a Wiener prediction-based method, Mahalanobis distance measure and subspace projection method. We compare the performance of these methods using multi-look SAR images containing several targets (mines). We present results in the form of receiver operating characteristics (ROC) curves.

Key-Words:- Change detection, mine detection, Wiener prediction, distance measures, SAR imagery

1 Introduction

Using multitemporal SAR images of the same scene, analysts employ several methods to determine changes among the set [1]. Change may be abrupt in which case only two images are required or it may be gradual in which case several images of a given scene are compared in order to identify change. The former case is considered here, where SAR images are analyzed to detect land mines. Much of the change detection activity has been focused on optical data for specific applications, e.g., several change detection methods are implemented and compared to detect land cover changes in multispectral imagery [2]. However, due to the natural limitations of optical sensors, e.g., sensitivity to weather and illumination conditions, SAR sensors may constitute a superior sensor for change detection as images for this purpose are obtained at various times of day under varying conditions.

In this chapter, we have implemented image differencing, ratio, Euclidean distance, Mahalanobis distance, subspace projection-based [3-4], Wiener filter-based change detection [5] and compared their performance to one another. We demonstrate all algorithms on co-registered SAR images obtained from a high resolution, VV-polarized SAR system. In Section 2, we discuss difference-based change detection, Euclidean distance, and ratio change detection methods which comprise the simpler change detection methods implemented in this paper. In Sections 3-5 we discuss more complex methods such as Mahalanobis distance, subspace projection-based change detection, and Wiener filter-based change detection, respectively. We consider specific implementation issues in Section 6 and present results in Section 7. Finally, a conclusion is provided in Section 8.

2 Difference, Euclidean distance, and image ratioing change detection methods

In simple difference-based change detection a pixel from one image (the reference image) is subtracted from the pixel in the corresponding location of another image (the test image) which has changed with respect to the reference image. If the difference is greater than a threshold, then a change is said to have occurred. One can also subtract a block of pixels from one image from the corresponding block from a test image. This is referred to as Euclidean difference if the blocks of pixels are arranged into vectors and the L-2 norm of the difference of these vectors is computed. We implemented the Euclidean distance as in (1) where we computed the L-2 norm of the difference between a block of pixels (arranged into a 1 dimensional vector) from reference

image, $\mathbf{f}_X$, and the corresponding block in the test image, $\mathbf{f}_Y$, to obtain an error, $e_E(i,j)$

$$e_E(i,j) = \left\| \mathbf{y}_{ij} - \mathbf{x}_{ij} \right\| \quad (1)$$

where $\mathbf{x}$ and $\mathbf{y}$ are vectors of pixels taken from $\mathbf{f}_X$ and $\mathbf{f}_Y$, respectively at location *(i,j)*. We display this error, $e_E(i,j)$, as an image. When no change has occurred this error is expected to be low and the error will be high when a change has occurred. While simple differencing considers only two pixels in making a change decision, the Euclidean distance takes into account pixels within the neighborhood of the pixel in question. This regional decision may have a smoothing effect on the change image at the expense of additional computational complexity.

Closely related to the Euclidean distance metric for change detection is image ratioing. In many change detection applications ratioing proved more robust to illumination effects than simple differencing. It is implemented as follows:

$$e_R(i,j) = \frac{y_{ij}}{x_{ij}} \quad (2)$$

where y_{ij} and x_{ij} are pixels from the same locations in the test and reference images, respectively.

3 Mahalanobis distance-based change detection

Simple techniques like differencing and image ratioing suffer from sensitivity to noise and illumination intensity variations in the images. Therefore, the Mahalanobis distance measure is used to detect changes in SAR imagery. In this change detection application, we obtain an error (change) image by computing the Mahalanobis distance between $\mathbf{x}$ and $\mathbf{y}$ to obtain $e_{MD}(i,j)$ as follows.

$$e_{MD}(i,j) = \sqrt{(\mathbf{x}_{ij} - \mathbf{y}_{ij})^T \mathbf{C}_X^{-1} (\mathbf{x}_{ij} - \mathbf{y}_{ij})} \quad (3)$$

The $\mathbf{C}_X^{-1}$ term in the Mahalanobis distance is the inverse covariance matrix computed from vectors of pixels in $\mathbf{f}_X$. By considering the effects of other pixels in making a change decision with the inclusion of second order statistics, the Mahalanobis distance method is expected to reduce false alarms. The $\mathbf{C}_X^{-1}$ term should improve the estimate by reducing the effects of background clutter variance which, for the purpose of detecting mines in SAR imagery, does not constitute a significant change.

4 Subspace projection-based change detection

In order to apply subspace projection to change detection a subspace must be defined for either the reference or test image. We computed the covariance of a sample from $\mathbf{f}_X$ and its eigenvectors and eigenvalues as follows:

$$\mathbf{C}_X = (\mathbf{X} - \boldsymbol{\mu}_X)(\mathbf{X} - \boldsymbol{\mu}_X)^T \quad (4)$$

where $\mathbf{X}$ is a matrix of pixels whose columns represent a block of pixels from $\mathbf{f}_X$, arranged as described in Section 6, having mean $\boldsymbol{\mu}_X = \mathbf{X}\mathbf{1}_{NxN}$. $\mathbf{1}_{NxN}$ is a square matrix of size NxN whose elements are 1/N, where N is the number of columns of $\mathbf{X}$. We define the subspace of the reference data, which we can express using eigen-decomposition in terms of its eigenvectors, $\mathbf{V}$, and eigenvalues, $\boldsymbol{\Lambda}$

$$\mathbf{C}_X = \mathbf{V}\boldsymbol{\Lambda}\mathbf{V}^T. \quad (5)$$

We truncate the number of eigenvectors in $\mathbf{V}$, denoted by $\tilde{\mathbf{V}}$, to develop a subspace projection operator, $\mathbf{P}_X$:

$$\mathbf{P}_X = \tilde{\mathbf{V}}\tilde{\mathbf{V}}^T. \quad (6)$$

The projection of the test image onto the subspace of the reference image will provide a measure of how much of the test sample is represented by the reference image. Therefore, by computing the squared difference between the test image and its projection onto the subspace of the reference image we obtain an estimate of the difference between the two images,

$$e_{SP}(i,j) = \sqrt{[\mathbf{y}_{ij}^T (\mathbf{I} - \mathbf{P}_X)\mathbf{y}_{ij}]}. \quad (7)$$

We evaluated the effects of various levels of truncation and display the best results achieved. In our implementations we include the $\mathbf{C}_X^{-1}$ term in the subspace projection error term as follows:

$$e'_{SP}(i,j) = \sqrt{\mathbf{y}_{ij}^T (\mathbf{I} - \mathbf{P}_X)^T \mathbf{C}_X^{-1} (\mathbf{I} - \mathbf{P}_X)\mathbf{y}_{ij}}. \quad (8)$$

We expect it will play a similar role as it does in the Mahalanobis prediction and further diminish false alarms by suppressing the background clutter.

5 Wiener prediction-based change detection

We propose a Wiener prediction-based change detection algorithm to overcome some of the limitations of simple differencing, namely to exploit the highly correlated nature of speckle noise, thereby

reducing false alarms. close to the actual data. The Wiener filter [5] is the linear minimum mean-squared error estimator for second-order stationary data. Consider the signal $\hat{\mathbf{y}}_{ij} = \mathbf{W}\mathbf{x}_{ij}$. The goal of Wiener filtering is to find **W** which minimizes the error, $e_W(i,j) = \|\mathbf{y}_{ij} - \hat{\mathbf{y}}_{ij}\|$, where **y** represents a desired signal. In the case of change detection **y** is taken from the test image, $\mathbf{f}_Y$, which contains changes as compared to the reference image, $\mathbf{f}_X$. The Wiener filter seeks the value of W which minimizes the mean squared error, e_W. If the linear minimum mean-squared error estimator of **Y** satisfies the orthogonality condition, the following expressions hold:

$$\begin{aligned} E\{(\mathbf{Y} - \mathbf{W}\mathbf{X})\mathbf{X}^T\} &= 0 \\ E\{\mathbf{Y}\mathbf{X}^T\} - E\{\mathbf{W}\mathbf{X}\mathbf{X}^T\} &= 0 \\ \mathbf{R}_{YX} - \mathbf{W}\mathbf{R}_{XX} &= 0, \end{aligned} \tag{9}$$

where $E\{\cdot\}$ represents the expectation operator, **X** is a matrix of pixels whose columns represent a block of pixels from $\mathbf{f}_X$, **Y** is a matrix of pixels from $\mathbf{f}_Y$ whose columns represent a block of pixels at the same locations as those in **X**, $\mathbf{R}_{YX}$ is the cross correlation matrix of **X** and **Y**, and $\mathbf{R}_{XX}^{-1}$ is the auto correlation matrix of **X**. For a complete description of the construction of **X** and **Y** see Section 6. The equations in (11) imply that **W** satisfies the Wiener-Hopf equation, which has the following solution:

$$\mathbf{W} = \mathbf{R}_{YX}\mathbf{R}_{XX}^{-1}. \tag{10}$$

Therefore, we have:

$$\hat{\mathbf{y}}_{ij} = \mathbf{R}_{YX}\mathbf{R}_{XX}^{-1}\mathbf{x}_{ij}, \tag{11}$$

where $\mathbf{R}_{YX} = \mathbf{Y}\mathbf{X}^T$ and $\mathbf{R}_{XX}^{-1} = (\mathbf{X}\mathbf{X}^T)^{-1}$. So the error can be computed as follows

$$e_W(i,j) = \|\mathbf{y}_{ij} - \hat{\mathbf{y}}_{ij}\|. \tag{12}$$

In a modified implementation of the Wiener prediction-based change detection method, we insert a normalization (or whitening) term, $\mathbf{C}_X^{-1}$, into the error equation as follows:

$$e'_W(i,j) = \sqrt{(\mathbf{y}_{ij} - \hat{\mathbf{y}}_{ij})^T \mathbf{C}_X^{-1}(\mathbf{y}_{ij} - \hat{\mathbf{y}}_{ij})}. \tag{13}$$

We expect it will play a similar role as it does in the Mahalanobis prediction and further diminish false alarms by suppressing the background clutter. In our work we implemented (13) to detect changes in pixels occurring from one image to another. e'_W (i,j) is the error at each pixel, which we display as an image.

6 Implementation considerations

In implementing the Mahalanobis distance, subspace projection based-, and the Wiener filter-based change detection methods, we constructed our data matrices and vectors locally in order to compute the local statistics and generate a change image. We generate **X**, **Y**, **x**, and **y** using dual concentric sliding windows. **X** and **Y** are matrices of pixels contained within an outer moving window (size mxm), whose columns are obtained from overlapping smaller blocks ($\mathbf{x_1}$, $\mathbf{x_2}$, …,$\mathbf{x_M}$ each of size nxn) within the outer windows of the reference image and test image, respectively, as demonstrated in Fig. 1 and Fig. 2 for **X** where $\mathbf{X} = [\mathbf{x}_1\ \mathbf{x}_2 \ldots \mathbf{x}_M]$. Accordingly, the dimensions of **X** and **Y** will be NxM, where $N=n^2$ and $M=m^2$. Note, for clarity the windows that generate the columns of **X** and **Y** are not shown as overlapping in Fig. 2. However, in actual implementation the **X** and **Y** matrices are constructed from overlapping windows within **X** and **Y**. **x** and **y**, as shown in Fig. 1, are Nx1 vectors composed of pixels within the inner window (size n x n) of the reference image, $\mathbf{f}_X$, and test image, $\mathbf{f}_Y$, respectively. In this local implementation we must compute the necessary statistics at each iteration as we move pixel by pixel through the image, thereby generating new **X** and **Y** matrices and **x** and **y** vectors.

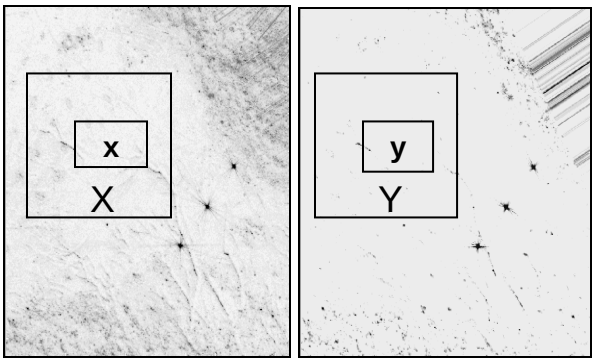

Fig.1 Dual Concentric sliding windows of the reference and test images, respectively.

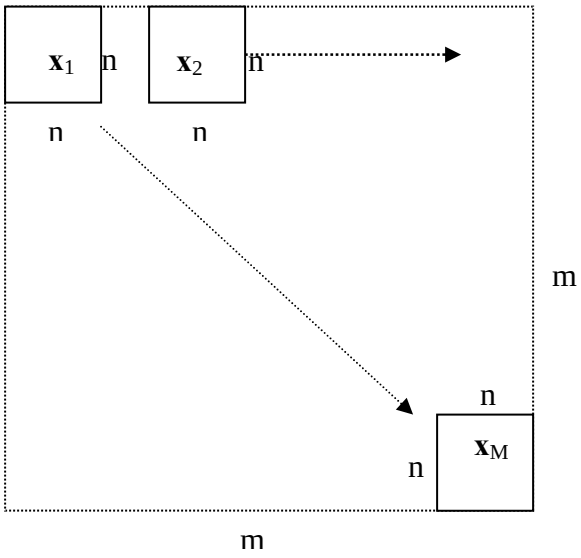

Fig.2 Construction of X matrix.

7 Experimental Results

Results from all methods implemented were normalized between zero and one before producing ROC curves. The threshold to generate the ROC curves also ranged from zero to one in increments of 10^{-3}. We used multi-look data collected at X band from a high resolution, VV-polarized SAR system (Fig. 3a and 3b). Small mines, comprising about a 5x5 pixel area, appear in the test image (Fig. 3b). The size of both the reference and test image is 950x950 pixels. Ground truth was provided which indicates the approximate center location of the known mines; we defined the mine area as an area slightly bigger than the average mine, centered at the locations indicated by ground truth information. To determine the performance, a hit was tabulated if at least a single pixel within the mine area surpassed the threshold. Any pixel outside of a mine area which surpassed the threshold was counted as a false alarm.

Fig. 4a shows the pixel differencing and Fig. 4b shows the Euclidean distance change images. The ratio change image obtained from (2) is represented in Fig. 5b. The local implementation results shown in Fig. 5b, 6a, and 6b are from implementations where the inner window was of size 3x3; the outer window, from which we constructed **X** and **Y** matrices to compute the second order statistics, was of size13x13. We gathered one hundred and sixty-nine overlapping 3x3 blocks from the 13x13 area, arranged each into a 9x1 vector, and placed them as columns in a matrix of size 9x169. We re-computed **X** and **Y** at each iteration to determine change at each pixel.

The three very bright spots in the original images, Fig. 3, are used to register the images and were identified as changes in the simple change detection methods. The local methods which incorporated image statistics were able to eliminate these bright areas from the change image (Figs. 5b, 6a, and 6b), as they are present in both the reference and test images at different intensities. Another area of the image which results in many false alarms after processing by the simpler methods, (results shown in Fig. 4a, 4b, and 5a), is the area in the upper right quadrant of the image. In the test image, Fig. 3b, this area is comprised of several slanted lines, while in the reference image, Fig. 3a, there is a more random, grainy pattern. The Wiener filter-based method with $\mathbf{C}_X^{-1}$, Mahalanobis distance, and subspace projection method with $\mathbf{C}_X^{-1}$ methods all show far fewer false alarms in this area than is shown in the results from the simpler change detection methods. ROC curves for the simple change detection methods can be seen in Fig. 7a and ROC curves for the more complicated methods which have the $\mathbf{C}_X^{-1}$ term are shown in Fig. 7b. A plot of the ROC curves for all the methods implemented is displayed in Fig. 8 for comparison.

Local Wiener with $\mathbf{C}_X^{-1}$, local Mahalanobis, local subspace projection with $\mathbf{C}_X^{-1}$, and ratio methods all show similar performance. However, the local Mahalanobis distance method begins to perform worst than the others from about .4 to .65 probability of detection (Pd) rate, then surpasses all the other methods above Pd = .65. The simple difference method has the worst performance over all Pd rates.

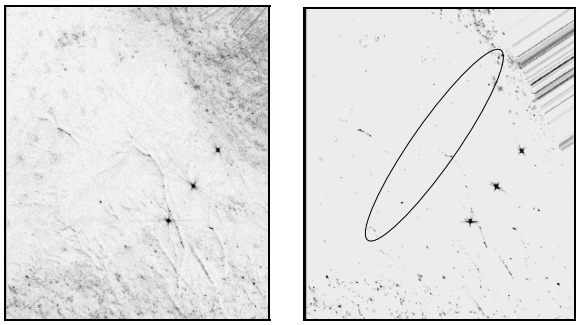

(a) (b)

Fig.3 Original SAR Images: (a) Reference image, (b) Test image with mines contained in elliptical area.

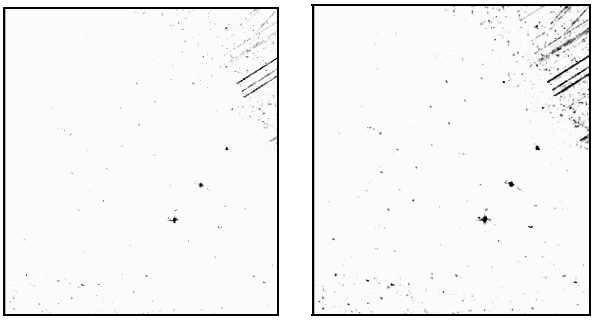

(a) (b)

Fig.4 (a) Simple difference change image, (b) Euclidean distance change image.

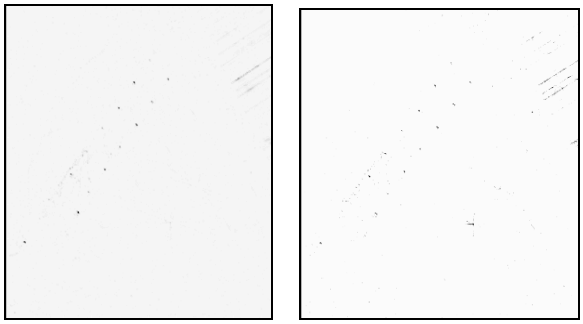

(a) (b)

Fig.5 (a) Ratio change image, (b) Local Mahalanobis distance change image.

(a) (b)

Fig.6 (a) Local Subspace Projection (with $\mathbf{C}_X^{-1}$ term) change image, (b) Local Wiener predicted (with $\mathbf{C}_X^{-1}$ term) change image.

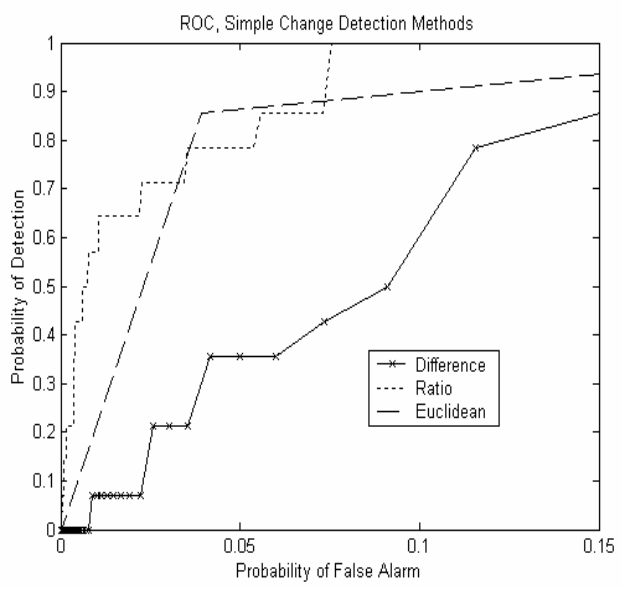

(a)

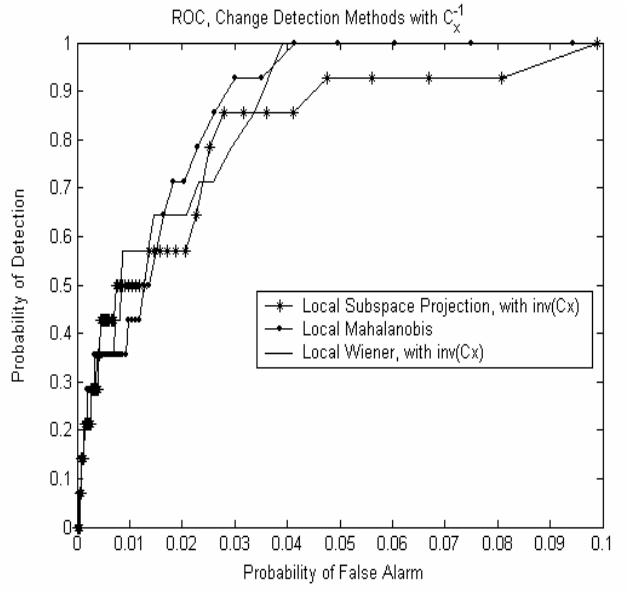

(b)

Fig.7 ROC curves displaying performance of (a) simple change detection methods and (b) methods incorporating $\mathbf{C}_X^{-1}$ term.

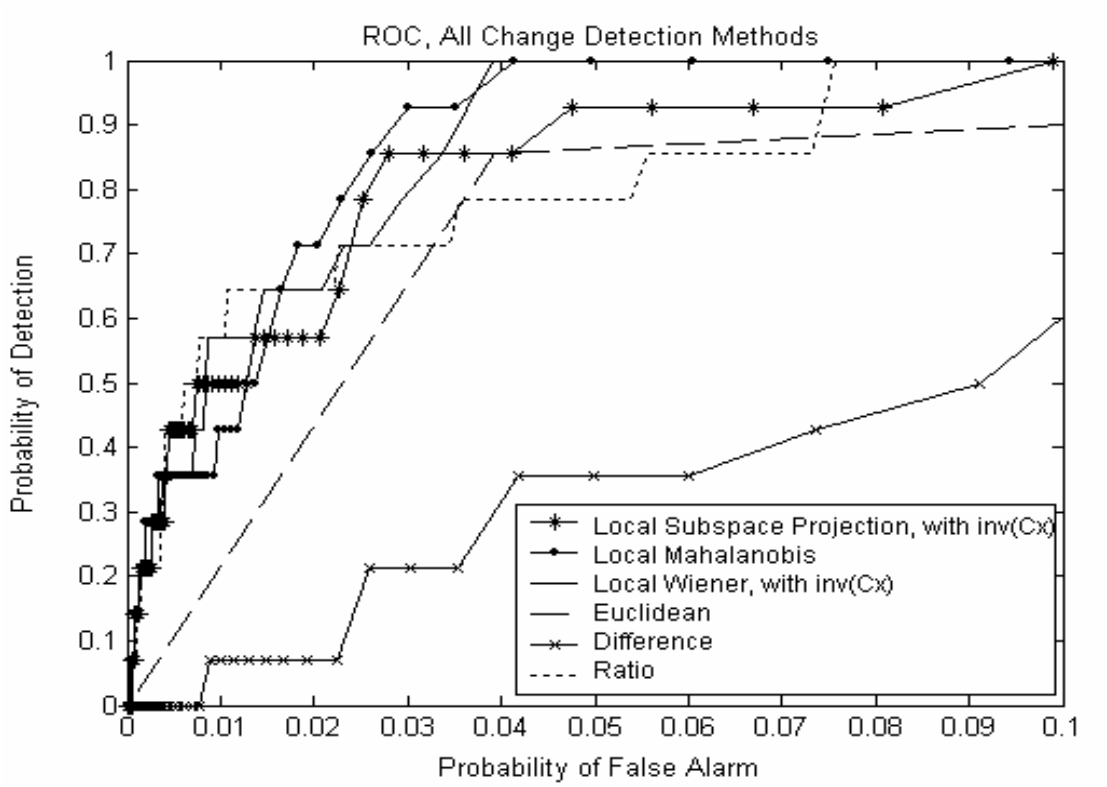

Fig.8 ROC curves displaying performance of the various change detection methods implemented in this paper.

8 Conclusion

As we have only demonstrated the algorithms on a limited data set of one scene, it is not prudent to make broad conclusions. However there are some trends indicated by the results above. Results above indicate that in general the more complex algorithms exhibited superior performance as compared to the simple methods; the exception seems to be the ratio method. The ratio method, although a simple implementation, has performance which is competitive with the more complex change detection methods implemented up to a Pd rate approximately equal to 0.65. Its performance degrades at higher detection rates, where it suffers from more false alarms than the methods which have the $\mathbf{C}_X^{-1}$.

Results indicate that taking into account the local spatial and statistical properties of the image improves the change detection performance. Local characteristics are used in computing the inverse covariance matrix, resulting in fewer false alarms as compared to the simple change detection methods. The ROC curves in Figs. 7 and 8 also show that addition of the $\mathbf{C}_X^{-1}$ term may serve to mitigate false alarms that arise from speckle which is a hindrance to achieving low false alarm rates with the Euclidean distance and simple difference methods. As expected the simple difference method exhibits the worst performance, having a high occurrence of false alarms.

References:

[1] R. J. Radke, S. Andra, O. Al-Kofahi and B. Roysam, "Image change detection algorithms: a systematic survey," IEEE Trans. Neural Networks, vol. 14, no. 3, 2005, pp. 294-307.

[2] J. F. Mas, "Monitoring land-cover changes: a comparison of change detection techniques," International Journal of Remote Sensing, vol. 20, no. 1, 1999, pp. 139-152.

[3] K. Ranney and M. Soumekh, "Adaptive change detection in coherent and noncoherent SAR imagery," Proc. of IEEE International Radar Conference, 2005, pp. 195-200.

[4] H. Kwon, S. Z. Der and N. M. Nasrabadi, "Projection-based adaptive anomaly detection for hyperspectral imagery," Proc. of IEEE International Conference on Image Processing, 2003, pp. 1001-1004.

[5] L. Scharf, Statistical Signal Processing: Detection Estimation, and Time Series Analysis, Addison Wesley, Colorado, 1991.